Research Square

Preprints are preliminary reports that have not undergone peer review.
They should not be considered conclusive, used to inform clinical practice,
or referenced by the media as validated information.

The role of shipping capacity and maritime regulation in ocean liming deployment

Marco Gambarini

marco.gambarini@cmcc.it

RFF-CMCC European Institute on Economics and the Environment (EIEE)

Lara Aleluia Reis

Euro-Mediterranean Center on Climate Change (CMCC) https://orcid.org/0000-0002-6676-7007

Cindy Giselle Azuero Pedraza

European Institute on Economics and the Environment

Hesam Naghash

Delft University of Technology

Laurent Drouet

RFF-CMCC European Institute on Economics and the Environment (EIEE) https://orcid.org/0000-0002-4087-7662

Article

Keywords:

Posted Date: August 14th, 2026

DOI: https://doi.org/10.21203/rs.3.rs-10430642/v1

License: This work is licensed under a Creative Commons Attribution 4.0 International License.
Read Full License

Additional Declarations: There is **NO** Competing Interest.

The role of shipping capacity and maritime regulation in ocean liming deployment

Marco Gambarini[1,2], Lara Aleluia Reis[1,2,4], Cindy G. Azuero-Pedraza[1,2], Hesam Naghash[3], Laurent Drouet[1,2,4]

[1] CMCC Foundation - Euro-Mediterranean Center on Climate Change, Via Marco Biagi 5, Lecce, 73100, Italy

[2] RFF-CMCC European Institute on Economics and the Environment, Via Solari 11, Milano, 20144, Italy

[3] Delft University of Technology, Delft, Netherlands

[4] CENSE – Center for Environmental and Sustainability Research & CHANGE - Global Change and Sustainability Institute, NOVA School of Science and Technology, NOVA University Lisbon, Campus de Caparica, 2829-516 Caparica, Portugal

Abstract

Ocean alkalinity enhancement (OAE), including ship-based ocean liming, has attracted attention as a potentially scalable carbon dioxide removal (CDR) method. OAE must therefore be represented in Integrated Assessment Models (IAMs) for long-term climate projection, especially in overshoot analysis. In this work, we present the implementation of ocean liming in the WITCH IAM, which integrates a detailed international shipping module, enabling explicit modeling of increased demand for advanced low-carbon engine technologies and fuels, and linking ocean liming to available port capacity. Our results indicate that under a stringent mitigation scenario with constrained shipping availability, ocean liming could reach 1 $GtCO_2$/yr around mid century, and provide 1.7—2.9 $GtCO_2$/yr of removals late in the century, corresponding to 9—15% of the total CDR portfolio. We find that deployment strongly depends on regulations about allowed sea areas and on the availability of low-carbon fuels in the long term.

1 Introduction

Limiting global warming to well-below 2°C, and pursuing efforts towards a 1.5°C target, is increasingly challenging without temperature overshoot. The remaining carbon budget for limiting the temperature increase to 1.5°C compared to preindustrial levels without overshoot will be depleted around 2028 (50% probability) [11]. In order to meet the most ambitious climate targets, massive efforts in carbon dioxide removal (CDR), on the order of 100 to 1000 tCO_2 over the 21st century, are considered necessary [4, 19]. In Paris-consistent pathways, CDR is needed to compensate for hard-to-abate emissions and to eventually reduce the atmospheric CO_2 concentration, bringing global temperature down after the overshoot. Large scale deployment of any CDR option raises sustainability, monitoring, reporting and verification issues, and logistical challenges.

It is thus important to assess and plan for a diversified portfolio of options, instead of relying on a single technology [6].

One of the potential CDR approaches considered in recent years is ocean alkalinity enhancement (OAE) and, in particular, ocean liming [31]. This technology relies on increasing the alkalinity of the ocean water to enhance its potential of sequestering CO_2 from the atmosphere and storing it in the form of carbonate and bicarbonate ions [30]. Alkalinity in seawater can be expressed approximately as in [35]:

$$Alk \approx [Na^+] + 2[Mg^{2+}] + 2[Ca^{2+}] + [K^+] - [Cl^-] - [Br^-] - [NO_3^-]. \quad (1)$$

In ocean liming, alkalinity is increased by adding Ca^{2+} ions through the release of hydrated lime, $Ca(OH)_2$, either from ships or along the shore. This addition quickly shifts the chemical equilibria of sea water and increases the pH [5]. As a result, a negative ocean-atmosphere p_{CO_2} gradient is established inducing a re-equilibration with the atmosphere that takes up CO_2. Atmosphere-sea water re-balancing is a slow process: a simple box model estimates the characteristic (e-folding) time to be approximately eight months [37, Sec. 1.6.3]. More detailed estimates with regional resolution, obtained from computational fluid dynamics simulations [16, 32], indicate longer times scales reaching several years in some regions.

In this work, we investigate how OAE deployment changes in overshoot pathways with a systemic approach that includes the interaction between the economic, energy, and climate systems. We develop an explicit representation of ocean liming within the WITCH IAM [7]. We rely on existing techno-economic estimates and previous works [5, 20, 31]. In comparison with previous literature, this paper advances the representation of OAE in IAMs by integrating the WITCH OAE module with a detailed international shipping module [26], capturing transport demand, port capacity constraints, and a rich set of engine and fuel technologies, including ammonia, methanol, and hydrogen. To address the risk of overconfidence in IAM assessments of CDR, as observed in case of BECCS (Bioenergy with Carbon Capture and Storage) [36, 2], we constrain the growth of the ocean liming industry using the cement industry as a proxy, as in [29]. This is motivated by the fact that the two share the extraction, grinding and calcination processes, as will be explained in the following sections. Constraining the scale-up of new technologies in IAMs using data of analogous industries has recently been explored in [21].

Our aim is to assess how much CDR ocean liming can deliver until the end of the century in overshoot pathways that require sustained negative emissions, and how its cumulative and peak deployment depend on system interactions, scale and growth constraints, and mitigation timing. We assess the sensitivity of OAE deployment to shipping availability, including port capacity limits, the use of existing versus dedicated ships, and the enforcement of international maritime decarbonization targets. We address trade-offs by examining to which extent large-scale OAE deployment increases maritime bunker fuel emissions in the absence of such regulations. Throughout the scenarios, OAE is in direct competition with other carbon dioxide removal and mitigation options, allowing us to explore how competition for geological carbon storage impacts the CDR portfolio.

2 Results

We consider scenarios with a 2020–2100 carbon budget of 800 $GtCO_2eq$.[1] All scenarios, described in table 1 and fig. 1, are based on a *Main* one, which features basic, conservative assumptions. In particular, it allows deployment only inside exclusive economic zones. Its variants are divided into three thematic groups: Lime supply, Shipping, and Earth system; counterfactual scenarios are also considered.

Scenario	**Variant**	**Assumptions**
Main	—	Dedicated ships Deployment only in EEZs Port utilization constraint (8) *Global CCS injection rate limit*: 5 $GtCO_2$/yr until 2050, 20 $GtCO_2$/yr after
Lime supply	Mining cap	$Q_{lime} \leq K_{cement}$ replaces (4)
	Electric	Electric calciners replace gas-powered ones
	Low CCS	*Global CCS injection rate limit*: 5 Gt CO_2/yr all years
Shipping	Max	Both existing and dedicated ships Deployment in EEZs and non-EEZs No port utilization constraint
	IMO target	Shipping sector decarbonization by 2050
	No NH_3	NH_3 remains below current policy
Earth system	Instant	Instantaneous uptake: $k \to \infty$ in (9)
Counterfactual	No OAE	No OAE in CDR portfolio
	No OAE/NH_3	No OAE in CDR portfolio NH_3 remains below current policy

Table 1: **OAE scenario variants**. Scenario variant groups. For all scenarios other than *Main*, assumptions are understood as variations with respect to *Main*. Each scenario is run with 3 mitigation timing variants: early, delayed and late, if feasible.

2.1 Carbon removal

In our *Main* overshoot scenario with early mitigation, a peak value of yearly global gross removals with OAE of 2.75 $GtCO_2$ is reached (see fig. 2), while the range of all Main variants is 1.7—2.9 $GtCO_2$, and the early maximum deployment overshoot scenario (*Max*) reaches a peak of 9.13 $GtCO_2$/yr. All of these values are well below the global limit of 13 $GtCO_2$/yr reported in [31]. The

[1] This is consistent with an end-of-century temperature target of 1.6°C (5th-95th percentile interval: [1.5–1.8]) [4, Table 3.1], possibly achieved after a period of overshoot through substantial net negative emissions, and as such it is an appropriate choice for assessing ambitious CDR measures.

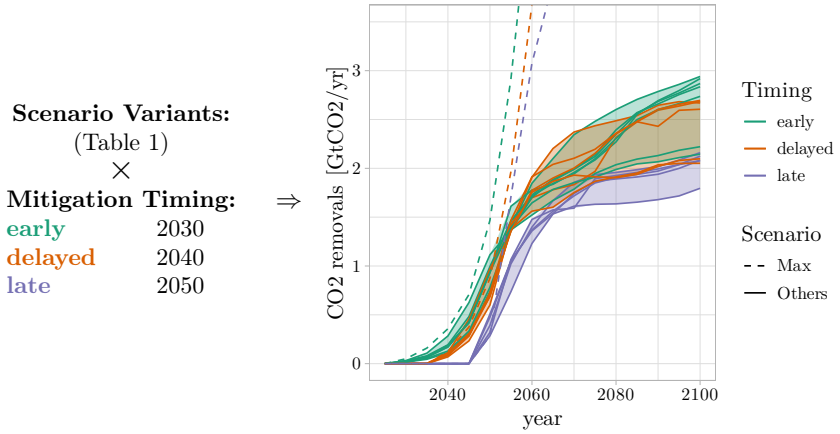


Figure 1: **Scenario matrix definition.** Each of the scenario variants from table 1 is combined with 3 mitigation timings, starting in 2030 (early), 2040 (delayed) and 2050 (late). Infeasible combinations are excluded from the analysis. On the right side, the chart presents the resulting CO_2 removals from ocean liming for all scenarios.

total gross removals from 2020 to 2100 are 114.66 $GtCO_2$ in the *Main* scenario and 360.38 $GtCO_2$ in the *Max* scenario, respectively. The scenario with the largest difference from the *Main* one is the *Max* scenario, which suggests that shipping volume constraints may be the most influential in determining total removals. This is confirmed by the results of the sensitivity analysis described in appendix B.2. The assumptions of limited mining growth (*Mining cap* scenario) and lower CCS availability also have a significant influence on the results, both in terms of yearly and cumulative removals. The assumptions of limited ammonia use for shipping, instantaneous capture, and IMO target achievement, lead to a very small variation with respect to the main scenario. Allowing the use of electric calciners instead of gas-fired ones has some effect on total removals, but a smaller one on peak yearly values.

Regarding the temporal dimension of scale-up, gross captures increase gradually, reaching 1 $GtCO_2$/yr between 2050 and 2065 in most scenarios (see the right panel of fig. 1). Early mitigation scenarios generally achieve 2 $GtCO_2$/yr between 2060 and 2080, while delayed and late scenarios mostly reach this value later in the century. With respect to the full CDR portfolio, shown in fig. 9 for several scenarios, we notice that total removals reach about 20 Gt/yr by the end of the century, about 10% of which is from OAE. This fraction is 9—15% across Main variants, and becomes more than a third in the early *Max* scenario.

Comparing results across mitigation timings (see the coloured dots in fig. 2) shows that a later start leads to both lower total removals and lower peak yearly removals. As discussed above, the *IMO target* scenario is not run for the late mitigation case, as its assumptions would not be well defined; this scenario also turns out to be infeasible in the delayed timing variant. Moreover, the *Low CCS*, late mitigation scenario is not feasible, meaning that the decarbonization and CDR options currently represented in WITCH are not sufficient for

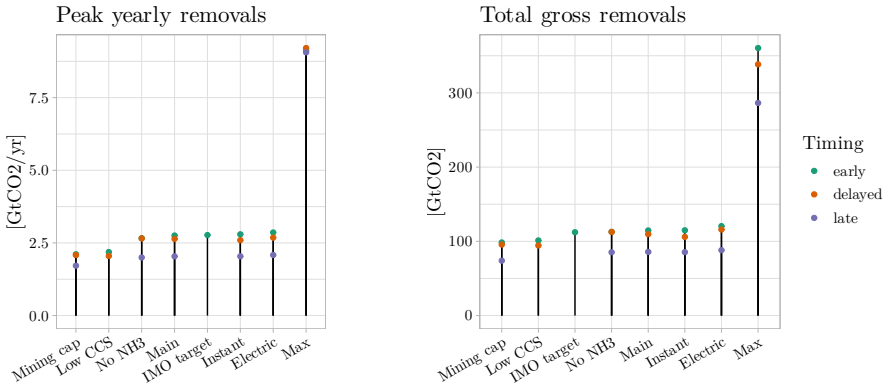


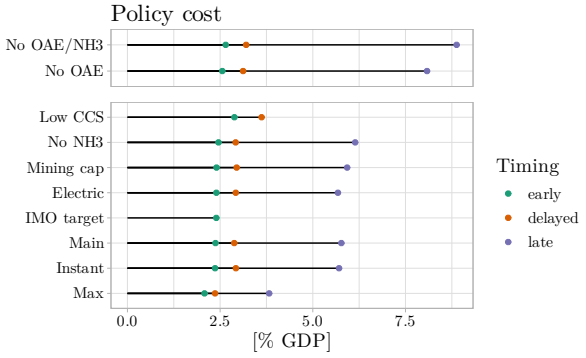
Figure 2: **Influence of the scenario variant on the CO_2 removal from OAE**. Left panel: maximum yearly removal expressed in $GtCO_2/yr$. Right panel: cumulative 2020–2100 total gross CO_2 removals from OAE. Scenario variants on the x-axis are ordered by increasing removals.

meeting the carbon budget prescribed if no additional action other than the current policies is done before 2050 and if massive CCS capacity is not available. The result that starting the deployment of additional mitigation measures later, and in particular OAE deployment, leads to lower total OAE removals is straightforward. However, also maximum yearly removals are generally lower in late decarbonization scenarios. This is because if mitigation is delayed, more stringent policies are required to meet the same carbon budget, resulting in a higher carbon tax. On the one hand, this promotes OAE deployment also in areas where it is less cost-effective (e.g., from ports farther from lime production plants, or in sea areas where efficiency is lower), potentially increasing its potential. On the other hand, as it leads to more costly options being deployed, it results in a significantly larger policy cost, as depicted in fig. 3a. This GDP decrease due to delayed action is reflected in a reduction of trade volume, see eq. (6), and consequently in lower limits of OAE deployment through the port capacity constraint (8); the value of such constraint is reported in fig. 16.

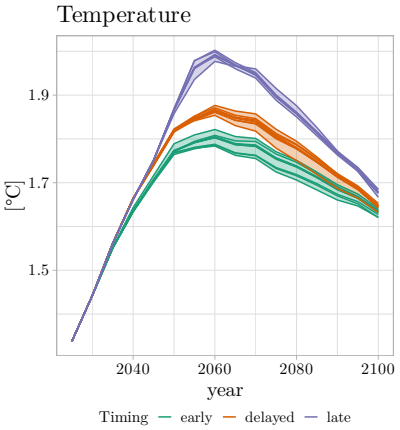
2.2 Policy cost and overshoot

We now focus on policy costs and on their possible tradeoffs with climate hazards. Figure 3a shows the policy cost, measured in terms of GDP loss with respect to the current policy scenario. We notice that adding the option of ocean liming to an overshoot scenario significantly decreases the policy cost associated to meeting the target with respect to the counterfactual, *No OAE* scenario, while a lower availability of CCS significantly increases it. The difference in policy cost between the scenario with the largest losses in the early timing case, *Low CCS*, and the one with the smallest losses, *Max*, is of the same order of magnitude as the average difference between the policy cost of early and delayed scenarios using the same OAE assumptions. Early and delayed scenarios all have policy costs below 4%, and mostly between 2% and 3.5%. For early Main variants, the policy cost reduction is around 7% compared to the *No OAE* scenario. Late mitigation scenarios, instead, have much larger costs, gen-

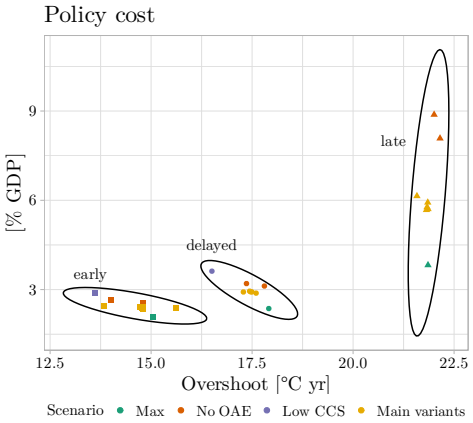
erally between 5% and 10% (with the only exception of *Max*). We observe that the variation in policy cost across assumptions in the late case is significantly larger than in the early and delayed case, and mainly determined by the scale and availability of OAE and ammonia.



(a) Policy cost by scenario variant.



(b) Temperature ranges.



(c) Temperature overshoot vs. mitigation cost.

Figure 3: **Mitigation cost and its relationship with temperature overshoot**. (a) Policy cost computed as the relative loss of cumulative, discounted global GDP over 2025–2100 with respect to the current policy scenario. (b) Temperature ranges: each single line corresponds to a scenario, while shaded areas highlight each timing's range across scenario variants. (c) Temperature overshoot, computed as the cumulative temperature exceedance of 1.5°C expressed in [°C·yr]; mitigation cost, computed as in (a). All temperatures computed using [22].

In these scenarios we have not taken into account climate damages in the utility functions that are optimized by coalitions. Temperature trajectories are reported in fig. 3b, and show that different mitigation timings have a significant effect on peak temperature, even when the total carbon budget (and thus, approximately, the end-of-century temperature) is the same: the difference in peak temperature between late scenarios and early scenarios is around 0.2 °C. This

implies than an additional contribution to GDP losses due to climate damages will be present in all scenarios, and more significantly in late mitigation ones.

To clarify this, in fig. 3c we report the policy cost of each scenario plotted against an overshoot indicator computed as the sum over years (from 2020 to 2100) of the exceedance of 1.5°C, namely

$$\sum_{i=t_0}^{t_f} \max(0, T_i - T_{ref}), \quad t_0 = 2020,\ t_f = 2100,\ T_{ref} = 1.5°\text{C}. \tag{2}$$

This indicator has been chosen for its simplicity and direct interpretability; more explicit connections with climate impact indicators are detailed in appendix B.3, where we show that the overshoot indicator is linearly correlated with a composite impact score over the scenarios of our interest. It is apparent from fig. 3b that overshoot severity increases with mitigation delay regardless of the other scenario assumptions. For early and delayed mitigation, *Low CCS* is the scenario with the lowest overshoot and the greatest policy cost, while OAE variants have a lower policy cost than *No OAE* scenarios and comparable values of the overshoot indicator. We can thus state that adding ocean liming to a CDR portfolio can reduce the policy cost in overshoot scenarios, without significantly increasing the climate risk related to overshoot.

2.3 Shipping sector impact

The fuel breakdown for the OAE shipping sector is shown in fig. 4: after the initial phase in which oil is mostly used, demand is met mostly by ammonia. An exception is the *Max* scenario, in which a substantial amount of oil is still used in 2060. Ammonia is indeed expected to be a significant contributor to decarbonization in future shipping scenarios [18, 25]; however, the almost total switch observed in our results, and driven by economic considerations, indicates that the model may require a more detailed representation of constraints and limitations of this fuel option. Regarding hydrogen, appearing in the *No NH_3* scenarios, it has been recognized that this fuel option is likely to be useful only for short routes due to frequent bunkering requirements [25]. This is consistent with the fact that in our scenario results dedicated ships for OAE are mostly in the small size category. Although the cost of transport per unit material carried is larger for small vessels compared to large ones, the former provide a better tradeoff for ocean liming, as the maximum amount of material that can be discharged per unit time is not assumed to scale linearly with deadweight tonnage, but rather with ship width.

In terms of emissions, adding the option of ocean liming increases total 2025-2100 emissions from international shipping by around 10% compared to the counterfactual *No OAE* scenario, with the exception of the *Max* scenario, for which increments are around 30% (see fig. 18). In general, shipping emissions are around 3% of total FFI emissions. Scenarios without ammonia have the highest bunker emissions and the greatest sensitivity of policy cost to mitigation timing (fig. 3a): delaying mitigation shifts the fuel mix from oil and traditional biofuels towards hydrogen, which is costly.

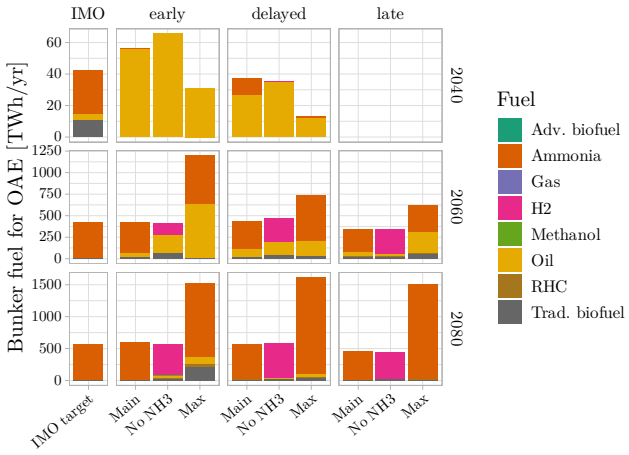


Figure 4: **Shipping fuel**. Bunker fuel consumption for OAE for scenarios relevant to shipping, across years. Note that the top right panel is empty as there is no OAE deployment in 2040 in the late scenario, as per assumptions. RHC refers to renewable hydrocarbons.

2.4 CCS and other feasibility barriers

Since the ocean liming process requires CCS and the capacity and injection rate of geological storage are limited, it is interesting to assess how scenario assumptions change the demand for it. In the *Main* scenario, power plants (e.g., BECCS plants) are the largest source of CO_2 to be stored at a global level (see fig. 12). This changes in the *Max* scenario, where calcination for OAE is the largest source while the other contributions are decreased. For these two scenarios, the profiles are comparable to the one reported in the CCS assessment of [13] for their below 2°C CCS breakthrough scenario. In the *Low CCS* scenario, the proportions of DAC, OAE and plant CCS are somewhat in the middle between the ones of the *Main* and *Max* scenarios. Shares of source vary widely across regions (see fig. 13), with Canada, USA, and Middle East and North Africa having a large proportion of DAC, and most others showing high shares of plant CCS. Even though the maximum injection rate limits are not reached at a global level, they are for several regions.

However, for most regions and in scenarios other than *Max*, OAE deployment is actually limited by either the port capacity constraint or the sustainability constraint, not by the CCS utilization constraint. As an example, in Figure 5 a comparison is shown between the amount of OAE performed, the sustainability limit, and the port constraint. We remark that the sustainability limit is only imposed on deployment from existing ships, which is restricted to exclusive economic zones: this is the reason why in the *Max* scenario the total deployment can exceed it. At least one of the two constraints is binding for all regions except for the Japan and Korea one. This changes in the *Low CCS* scenario (see fig. 14), where several regions use CCS exclusively, or almost exclusively, for OAE, and exhaust their CCS budget. This explains why shipping limits are likely to have a larger influence on OAE than CCS limits, as already observable from fig. 2, except when CCS limits are severely reduced.

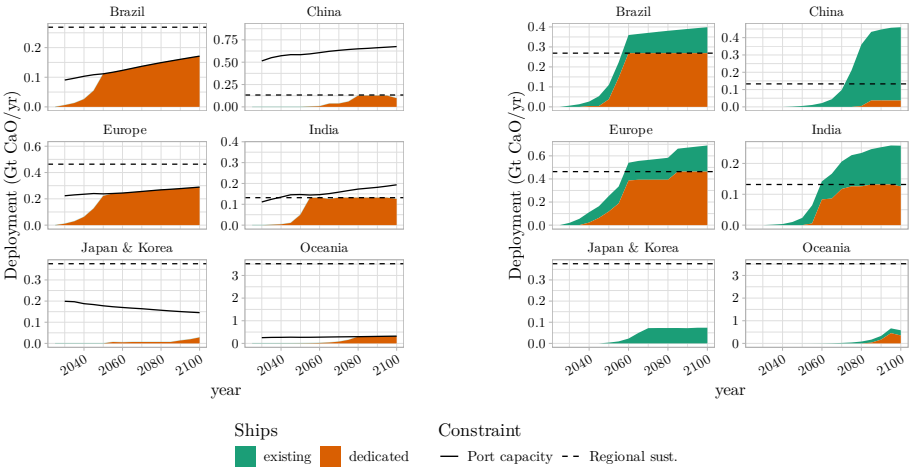


Figure 5: **Environmental sustainability and trade volume constraints.** Deployment in the *Main* (left) and *Max* (right) overshoot scenarios (coloured areas), sustainability limit (dashed lines) and port capacity constraint (solid lines). The sustainability limit is obtained by multiplying each region's EEZ area by 1.5 mol $Ca(OH)_2/(m^2/yr)$, see appendix A.1. A selection of regions is shown for clarity; the full results are reported in fig. 19 and fig. 20.

We finally comment about electricity demand (see fig. 21). For the early mitigation variant, in the *Main* overshoot scenario, electricity consumption is around or below 2% of the total in most regions; this is the least electricity-intensive scenario of the three. Moving from the *Main* to the *Max* and *Electric* scenarios, the electricity consumption fraction grows for all regions. In particular, it exceeds 10% of the total consumption for Indonesia in the *Max* scenario, Japan and Korea in the *Electric* scenario, and Oceania in both scenarios. This last region has overall very high values compared to the others, but still below 10% in the *Main* scenario.

3 Discussion

Our scenarios indicate that if the goal of meeting a carbon budget of 800 $GtCO_2e$ is pursued, with additional efforts on top of the current policies starting by 2030, and where up to 20% of the total port traffic can be dedicated to OAE limiting deployment to EEZs, the potential of this CDR option can grow to more than 1 $GtCO_2$ per year between 2050 and 2060, and to around 2.75 $GtCO_2/yr$ by the end of the century, representing more than 10% of the yearly carbon removals. The end-of-century deployment values found in this work are generally within the 1.8—9.1 $GtCO_2/yr$ range of the more constrained scenarios of the previous IAM assessment of [31], and all significantly smaller than the 18.5 $GtCO_2/yr$ of their default scenario.

Regarding the effects of system interactions and constraints, we find that the potential of ocean liming depends most significantly on shipping-related assumptions. The associated additional demand for shipping has effects on

emissions and fuel consumption. In high deployment scenarios, shipping CO_2 emissions increase by up to 30% compared to a counterfactual scenario. With respect to fuel demand, we find that in early stages of the technology it is satisfied by oil, and later by ammonia. In case the adoption of ammonia is blocked or severely limited for exogenous reasons, demand can be mostly met by hydrogen, a more expensive option. As expected, the potential of ocean liming also depends significantly on CCS availability: in the *Low CCS* scenario, cumulative removals are more than 10% lower than in *Main*. In our scenarios, several regions reach their CCS injection limits, and in *Max* around half of the CCS capacity is used for OAE.

Mitigation timing is an important driver of our results too. A delayed mitigation with the same carbon budget requires more stringent policies, as exemplified by the extreme carbon tax values of the late mitigation scenarios. It also requires more CDR deployment, and results in significantly greater GDP losses and dependence on CCS and advanced shipping fuels, making decarbonization pathways less robust. Incidentally, a lower GDP is linked to reduced international trade and thus port infrastructure growth, influencing our results on OAE potential. While the introduction of novel CDR options such as OAE can reduce the policy cost of meeting ambitious end-of-century carbon budgets, this means that with the same carbon budget there will be more emissions early in the century because of the anticipated potential to capture more carbon in later decades. We find that in the case of ocean liming this does not sensibly influence the total climate risk over the 21st century, as described by the overshoot indicator introduced in fig. 3c and discussed in appendix B.3.

A limitation of the presented analysis is the fact that carbon uptake by the ocean is computed assuming time-invariant coefficients. While the values reported in [38] and used here are obtained as difference with respect to a counterfactual scenario without OAE, which guarantees no double-counting of naturally occurring fluxes, the assessment is done for past years. An improvement would be obtainable by coupling with an Earth model of intermediate complexity, such as [9], which would allow to take into account the response of the ocean to an atmosphere with scenario-based CO_2 concentrations. A more detailed representation of physical processes related to OAE would also enable the estimation of spillovers between regions, due to the fact that even if deployment is confined to a region's EEZ, effects on chemical indicators can be observed in other regions' sea areas, with possible policy implications.

Finally, further developments of this work include the representation of other variations of OAE other than ship-based ocean liming, such as coastal-based deployment and the use of different minerals with the associated supply chains. Moreover, coupling OAE with an explicit cement module would enable a more detailed study of the scaleup phase and of the involved tradeoffs.

Acknowledgements The research leading to these results has received funding from the European Union's Horizon Europe research and innovation programme under the UPTAKE project (g.a. no. 101081521), the ELEVATE project (g.a. no. 101056873) and the OAeSIS project (g.a. no. 101289318). Views and opinions expressed are however those of the author(s) only and do not necessarily reflect those of the European Union. Neither the European Union nor the granting authority can be held responsible for them.

A Methods

A.1 Rationale and main equations

In this section we describe our model of ocean liming. The process is summarized in fig. 6. Quicklime (CaO) is produced from calcination of limestone ($CaCO_3$) and transformed by hydration into slaked lime ($Ca(OH)_2$), which is then distributed from ships. Calcination is described by the reaction

$$CaCO_3 + \text{heat} \rightarrow CaO + CO_2, \tag{3}$$

where heat can be provided either by gas combustion or by electricity. As seen from the reaction, this step always comes with a CO_2 output (and thus a possible demand for CCS), even if an electric calciner is used. In the following, we will call process emissions the ones due to the reaction itself, computable from stoichiometric coefficients and independent of the heat source used.

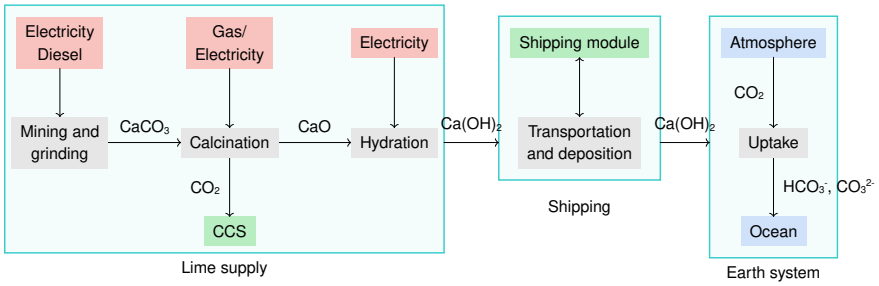


Figure 6: **Schematic of the ocean liming process.** Red boxes in the diagram refer to explicitly modeled energy inputs, green boxes to links to other WITCH modules, and blue boxes to Earth system elements.

Techno-economic assumptions about the process of transforming limestone into hydrated lime, including costs and energy demand, are taken from [20]. In particular, we assume that an oxy-fuel calciner fed by natural gas is used, and that both process emissions and emissions due to gas combustion are captured and stored with 95% efficiency. In WITCH, CCS injection rate limits are imposed as scenario-dependent values and allocated to regions based on the capacity distribution reported in [14]. Total storage capacity data per type of reservoir is from [17, 15].

The production process of hydrated lime described above is analogous to the one used in cement production. To obtain a plausible scale-up phase of OAE, we therefore impose a constraint on the absolute value and growth rate of lime production based on the cement industry dataset provided in [33]. We assume that each region can immediately utilize a fraction $\alpha = 0.1$ of its cement production capacity, K_{cement}, for the OAE industry. This figure is conservative compared to the difference between capacity and production reported in [33, Table 2], which is between 41% and 60% for the macro-regions considered therein. Following [29], we then assume a maximum annual growth rate $r_{lime} = 0.15$ for the mass of lime produced per year $Q_{lime}(t)$:

$$Q_{lime}(t) \leq \max(\alpha K_{cement}, (1 + r_{lime})^{\Delta t} Q_{lime}(t-1)), \tag{4}$$

where Δt is the length of each time period (in WITCH, $\Delta t = 5\text{yr}$). The sensitivities to coefficients α and r_{lime} are assessed in appendix B.2. We find small sensitivity of total and yearly OAE removals to α. With respect to r_{lime}, its reduction has a sensible effect on removals, while its increase has limited impact, likely due to the prevalence of other constraints. Considering the implementation into a gradient-based nonlinear optimization solver, the maximum operator in (4) is replaced by a smooth approximation. Land transportation distances from cement plants to the nearest ports are computed by country as detailed in appendix A.5; plant capacities are aggregated by port distance class. Equation (4) is applied separately for each region and transport distance class. This means that every region can initially produce lime up to a quantity equal to a fraction α of the current cement production capacity in each transport distance class. In the following time periods, regions are free to choose in which transport distance bin to increase their capacity and to which extent. The minimum cost solution is to saturate the constraint for the first transport distance class before moving on to higher distances. Emissions from land transportation are accounted for through the endogenous emission factor of freight vehicles, which takes into account possible electrification of the transport sector.

After calcination, lime is converted into hydrated lime by hydration, a process requiring water and electrical power. In our implementation, we take into account the electricity demand, but not the water demand. We will denote the total quantity of hydrated lime produced (and discharged from ships) per year simply as Q. Distribution of the material can be done either from a dedicated fleet of ships built specifically for OAE, or from existing vessels. We accordingly define quantities Q_{existing} and $Q_{\text{dedicated}}$. The implementation is connected to the maritime bunkers module of WITCH [26]. This module distinguishes between tanker ships, bulk carries and container ships, allows for 4 size classes, detailed in appendix A.6 for bulk carriers, and for different engine and fuel options. These include internal combustion engines, namely gas, diesel (allowing also for biofuels and renewable hydrocarbons), ammonia, and methanol, and hydrogen-powered fuel cells. We assume that dedicated ships for OAE have the same costs, size classes and fuel consumptions as bulk carriers [5], and the same lifetime of 22 years. International trade is computed using a gravity model [26]: the total mass of imports to region n_{dest} at time t, $T_{\text{import}}(t, n_{\text{dest}})$, is

$$T_{\text{import}}(t, n_{\text{dest}}) = T_0(n_{\text{dest}}) \cdot \text{GDP}(t, n_{\text{dest}})^{\beta_1} \cdot p_{\text{fuel}}(t, n_{\text{dest}})^{\beta_2}, \tag{5}$$

where $T_0(n_{\text{dest}})$ is a baseline coefficient related to the importing (destination) region, $p_{\text{fuel}}(t, n_{\text{dest}})$ is a fuel price indicator, and β_1, β_2 are calibrated elasticities. Then, the trade mass from region n to region n_{dest} is computed as

$$T(t, n, n_{\text{dest}}, s) = T_{\text{import}}(t, n_{\text{dest}}) \cdot a_{\text{orig}}(t, n, n_{\text{dest}}) \cdot a_{\text{size}}(n, n_{\text{dest}}, s), \tag{6}$$

where $a_{\text{orig}}(t, n, n_{\text{dest}})$ is a normalized allocation factor to exporting (origin) regions which depends on their GDP and $a_{\text{size}}(n, n_{\text{dest}}, s)$ is a normalized allocation factor to ship sizes, based on sea distances between regions. The costs of ship building and fuel are allocated to regions at an aggregated level based on an importer-pays principle. In [5] it was reported that between 10% and 20% of the net cargo capacity of existing container ships could be used for ocean liming. We call β this available fraction of capacity, and allow each region n to use existing ships on the outbound routes to region n_{dest} only up to a limited

mass of material:

$$Q_{\text{existing}}(t, n, n_{\text{dest}}, s) \leq \beta T(t, n, n_{\text{dest}}, s) \max\left(1, \frac{\sum_{n_{\text{orig}}} T(t, n_{\text{orig}}, n, s)}{\sum_{n_{\text{dest}}} T(t, n, n_{\text{dest}}, s)}\right), \tag{7}$$

where index s denotes the ship size category, T is the total trade mass from (6), and factor β is set to 0.15. The last term is a weighting factor that takes into account the fact that, on average, inbound ship capacity must be equal to outbound capacity, so that regions with a negative trade balance (more imports than exports) are not artificially penalized. Moreover, as massive deployment of ocean liming would likely require substantial new port facilities in addition to ships, we limit the total deployment (including existing and dedicated ships) to a fraction γ of the total, endogenous trade volume:

$$\sum_{n_{\text{dest}}, s} Q_{\text{existing}}(t, n, n_{\text{dest}}, s) + \sum_{s} Q_{\text{dedicated}}(t, n, s) \leq \gamma \max\left(\sum_{n_{\text{orig}}, s} T(t, n_{\text{orig}}, n, s), \sum_{n_{\text{dest}}, s} T(t, n, n_{\text{dest}}, s)\right). \tag{8}$$

We set $\gamma = 0.2$ in our main scenarios (see table 1) and assess the different values of this parameter in a simple sensitivity test (see appendix B.2). Dedicated ships for OAE and fuel consumption are allocated to regions based on an exporter-pays principle, so that each region is responsible, and pays, for the full process chain of ocean liming that it deploys.

An important concern related to OAE deployment is the potential precipitation of calcium carbonate, which can occur due to excessive release and lead to severely decreased CO_2 uptake [24, 5]. For this reason, we impose a maximum discharge rate from each ship. We assume that within the precipitation timescale of calcium carbonate, which is $\sim 10^3$ s [23, 5], the released material is well-mixed in the ship's wake. The cross-sectional wake area is approximated as the product of the ship's width and of a representative height of the mixed layer, which we take to be equal to 2 m, consistently with the value used in [20]. The maximum amount of material that can be discharged per unit time from a ship is then the product of the wake's representative area, of the ship's speed, and of the maximum safe concentration, whose values we take from [20].

In the model, we assume that the regional, dedicated fleets of OAE ships can deploy ocean liming inside their own exclusive economic zones (EEZ), while this limitation is not enforced for deployment from existing ships. EEZ maps have been retrieved from [10] and aggregated to the WITCH regions by territorial proximity (as opposed to sovereignty). This is consistent with the fact that WITCH regions aggregate, for example, overseas territories of European countries, which may have small land areas but give a substantial contribution to the area of the EEZ, based on their geographical location, not on sovereignty. OAE requires substantial transport of material from the mining and processing site to the sea, so retaining geographical contiguity inside regions is important. In [16], regional limits of OAE deployment are proposed, based on limiting the increase of pH to 0.1, which is of the same order as the ocean's acidification since preindustrial times, and on avoiding carbonate precipitation. This complements the limit on discharge from ships by adding an environmental sustainability component related to the pH. We remark that larger spikes in pH are anyway expected

to temporarily occur in ship wakes [5]. We take 3 mol Alk/(m^2/yr) as a conservative upper bound on the deployment rate, based on [16, Figure 2(b)]. Since each mole of $Ca(OH)_2$ provides two moles of alkalinity, the limit corresponds to 1.5 mol $Ca(OH)_2$/(m^2/yr).

Finally, we describe our modeling of uptake dynamics. Let $Q(t)$ be the deposition rate of calcium hydroxide (Gt/yr), $M(t)$ the mass of material available for reaction at time t (Gt) and $W(t)$ the total mass of material reacted in $[0, t]$ (Gt). $M(t)$ increases with deposition and decreases with reaction. The uptake process is described by the following system of linear ordinary differential equations:

$$\begin{cases} \dot{W}(t) = kM(t) & \text{(9a)} \\ \dot{M}(t) = Q(t) - kM(t) & \text{(9b)} \\ M(0) = M_0, \quad W(0) = W_0, & \text{(9c)} \end{cases}$$

together with the equation describing the amount of carbon captured $C(t)$,

$$C(t) = \eta W(t). \tag{10}$$

The spatial distributions of the reaction rate k and efficiency η are obtained by post-processing the results of [38] as explained in appendix A.3. System (9) admits an exact solution. In particular, assuming constant deposition $Q(t) = Q_j$ over a time step $[t_j, t_{j+1} = t_j + \Delta t]$, we have

$$M(t+1) = M(t)e^{-k\Delta t} + \frac{Q(t)}{k}\left(1 - e^{-k\Delta t}\right), \tag{11}$$

$$W(t+1) = W(t) + \left(1 - e^{-k\Delta t}\right) M(t) + Q(t)\Delta t - \frac{1 - e^{-k\Delta t}}{k} Q(t). \tag{12}$$

A.2 Extended scenario description

In this sections we provide additional details about our scenario setup, depicted in table 1 and fig. 1. Scenarios in the lime supply group aim to assess the limits of OAE in case the lime industry is limited to the current size of the cement industry, the efficiency increases and energy system implications of using electric calciners, and the effects of more prudent CCS assumptions. Shipping scenarios include the possibility of deployment outside EEZs from existing ships, increasing potential but requiring international governance, and explore the results of an enforcement of IMO targets and of the possibility that the adoption of ammonia is severely limited due for example to safety reasons [8] or air pollution concerns linked to storage and bunkering leaks [28]. The response of the Earth system is investigated in the *Instant* scenario where, instead of using physical values of the reaction rate k, a fictitious value is used, corresponding to having 99% of the total captures in the same time period of material deposition. Finally, counterfactual scenarios allow a comparison in terms of policy requirements with a future in which OAE does not scale up.

As shown in fig. 1, we consider 'early', 'delayed' and 'late' mitigation scenarios, where current policy trends are maintained until 2030, 2040 and 2050, respectively. After that, more ambitious mitigation policies are introduced, in the form of a linearly increasing carbon tax adjusted in order to meet the prescribed budget, as detailed in appendix A.4. The *IMO target* scenario is not run

in the late decarbonization case, as its target year coincides with the time period of mitigation start. In each case, WITCH is run in noncooperative mode, with 17 coalitions. Additional sensitivity scenarios devised to assess the influence of the assumed parameters α, r_{lime} and γ are presented in appendix B.2 Finally, a current policy scenario is run, in which no additional mitigation actions other than the ones already in place are considered (in particular, ocean liming is not deployed). This is used as a baseline for the computation of policy costs and for the ammonia level in the *No NH_3* and *No OAE/NH_3* scenarios.

A.3 Uptake efficiency and timescale aggregation

In [38], numerical pulse experiments are performed for 690 ocean regions and 4 months, each one representative of a season. The results are provided as time series of captured CO_2. In order to use this data in (11) and (12), we first average over the injection month. Then, we take as efficiency η the last value of the season-averaged time series. To obtain an equivalent reaction rate k, we first identify t90p, the time at which 90% of η is reached, and then consider an exponential curve of the form

$$x(t) = \eta(1 - e^{-kt}) \tag{13}$$

from which

$$k = -\frac{1}{\text{t90p}} \ln(1 - 0.9). \tag{14}$$

While in [38] a model with two separate timescales is suggested, we choose this simpler expression because of the limited, 5-year time resolution of WITCH, which is typical of IAMs. Using k-means clustering, 5 classes of efficiency and of time scale are identified, as shown in fig. 7. Finally, the regions of [38] are intersected with EEZ areas, obtaining, for each region, the amount of available ocean area in each efficiency and timescale bin. For the deployment from existing ships, that is modeled as completely taking place outside EEZs, we use as timescale the median timescale from the data of [38], and as efficiency the value 0.9 $tCO_2/tCa(OH)_2$, the central estimate of [20], that is more conservative than the median value of [38].

A.4 Carbon tax adjustment algorithm

In order to enforce a carbon budget in scenarios, the carbon tax is described by a global linear profile

$$\text{ctax}_{glob}(t) = \text{ctax}_{glob,0} + v_{ctax}(t - t_{ctaxstart}), \tag{15}$$

and regional carbon taxes are assumed to converge linearly to this profile from their initial values. The slope v_{ctax} is computed through an iterative process by applying, at each Nash (fixed-point) iteration, the update rule

$$v_{ctax}^{k+1} = v_{ctax}^{k} \left(1 - \frac{B_t - B_s}{\theta_1 - B_s}\right)^{\theta_2}, \tag{16}$$

where B_t is the total available carbon budget for the scenario, B_s is the spent carbon budget (total GHG emissions), k is the index of the Nash loop iteration, and θ_1, θ_2 are tunable coefficients. Additional safeguards are added to limit changes through iterations.

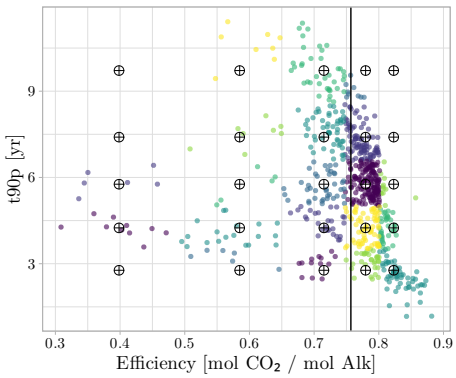


Figure 7: **Distribution of efficiencies and timescales**. Clustering of data points from [38]. Each colored dot corresponds to an ocean region in the assessment, black crossed circles are cluster centers and the vertical line corresponds to the efficiency estimate used in [20].

A.5 Road transport distance

Ports in [1] are first filtered based on the typical draft of handysize bulk carriers[2], the smallest ships considered in this study: only ports with cargo pier depth and/or maximum vessel draft larger than 9 m are considered. Then, for each cement plant in [33], we consider the closest port belonging to the same ISO3 country based on great circle distance. The road distance is computed using the OSRM API [27]. The plant-port pairs are then aggregated to distance classes, with bounds (0, 10, 25, 50, 100, 250, 500, 1000, max) km, where max denotes the mutual distance of the farthest pair; i.e., for each distance class and WITCH region, the total plant capacity reachable within a certain distance of any port is computed. The center of each interval is used as representative distance for the corresponding class. The result of this transport distance analysis for 4 representative countries is shown in fig. 8.

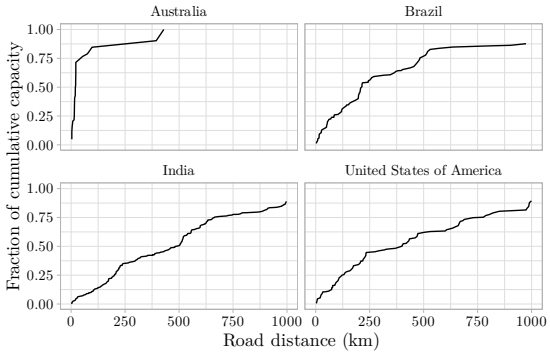


Figure 8: **Transport distance curves** between suitable ports and cement plants.

[2] `https://www.marbrokers.com/ship-types/handysize`

A.6 Ship size categories

The ship size categories used in this study are summarized in table 2. The key value is the width, used for the maximum discharge assessment.

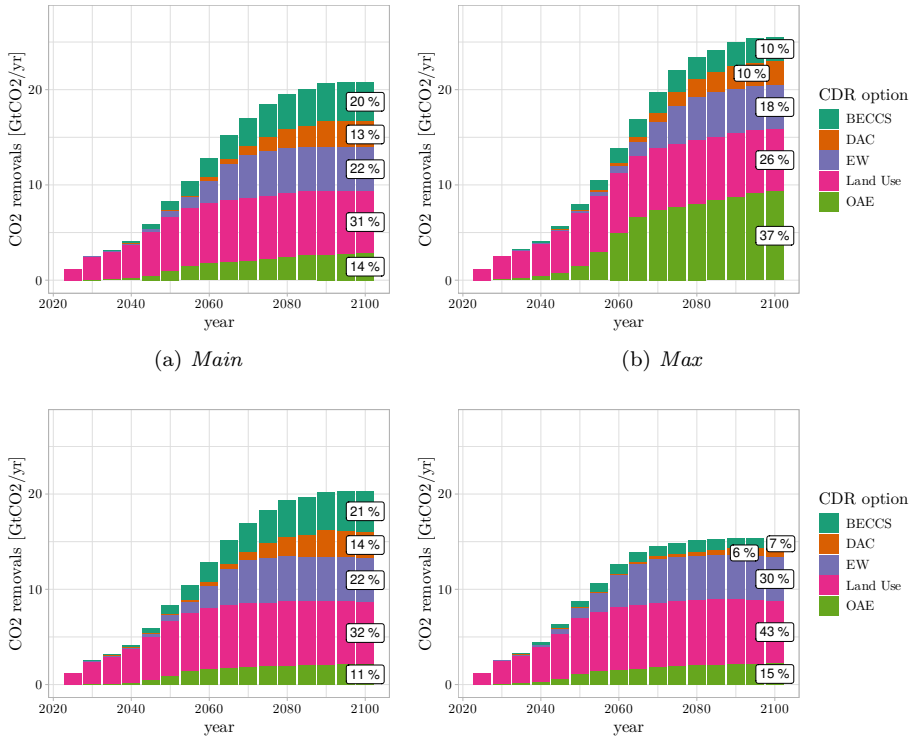
Size category	DWT Range	Description	Repr. length×width (m)	Repr. DWT
Small	0–35,000	Handysize vessels.	175×25	17,500
Medium	35,000–60,000	Handymax vessels.	175×31	47,500
Large	60,000–80,000	Panamax vessels.	294×32.3	75,000
Ultra-large	80,000+	Capesize and Bigger vessels.	290×45	100,000

Table 2: **Bulk carrier size categorization information**. Sources: `https://www.marbrokers.com/ship-types/handysize`, `https://www.clarksons.com/glossary/a-guide-to-bulk-vessel-sizes/`. DWT = Deadweight tonnage.

B Additional results

B.1 Details on scenarios from the main text

In fig. 9 we show the CDR portfolio in some of the early scenarios. The main effect of removing port capacity constraints and allowing OAE operations from existing ships is, as expected, an increase of the total removals, observed between the *Main* scenario and the *Max* scenario. A secondary effect is the decrease in magnitude of DAC and bioenergy: this is related to the switch in the shares of CCS sources already shown in fig. 12. Moving to the *Low CCS* scenario, the total amount of CDR is reduced compared to the *Main*, with a decrease of BECCS, DAC and OAE, which depend on CCS, and an increase of the other options, caused by the carbon tax increase required to meet the same budget.



(a) *Main* (b) *Max*

(c) *No NH_3* (d) *Low CCS*

Figure 9: **CDR portfolio in early overshoot scenarios.** Labels inside the figure refer to the share of each option with respect to the total in 2100.

Figure 10 shows the positive process emissions per unit lime production for the early mitigation *Main* and *Electric* scenarios. We choose to use lime production as a denominator instead of gross captures because the latter are delayed (according to the equations in system 9) with respect to the time when process emissions are released, that is when lime production happens. The results can be interpreted taking into account that 1 ton of lime (CaO) leads to the capture of about 1 ton of CO_2 [12]. In the initial years, efficiency of the

process is around 85% and the largest contribution is due to shipping, as mainly oil-powered diesel ships are initially used. Later, decarbonization of the shipping fleet and of the electricity supply takes place and is virtually completed around 2070. After that, the dominant contribution is the fraction of emissions from the calciner that are not stored, and efficiency is close to 95%. Emissions due to road

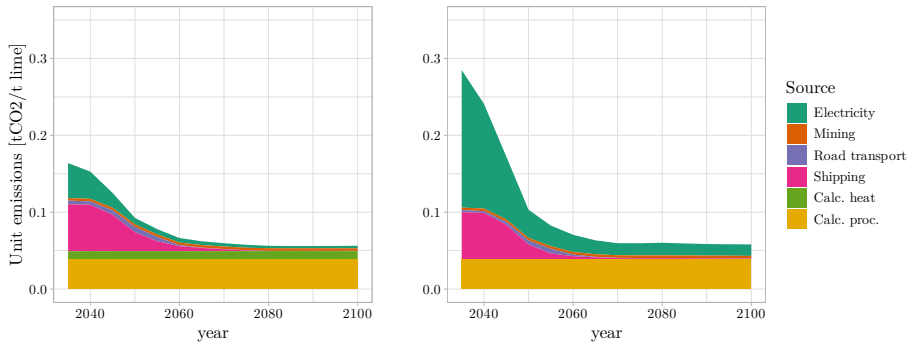


Figure 10: **Process emissions.** Breakdown of contributions to the process emissions of OAE by source, early *Main* scenario (left) and early *Electric* scenario (right).

transportation are small compared to the total, and they slightly increase at the start before decreasing again. This is because of the scaleup constraint, which limits the amount of lime that can be immediately sourced from the closest distance class, requiring regions to temporarily utilize farther plants to meet demand (see fig. 11). These results can be compared to the life cycle assessment presented in [12]. Their findings range from about 55% efficiency assuming the current technology and electricity mix and no geological storage of the calciner's heating emissions, to full efficiency with negative process emissions in the most optimistic case, in which heat recovery from the calcination process provides additional avoided emissions. We point out that [12] are using a significantly lower assumption for ship transport distance than we do, as they account for a 0.37 km ship transport distance per ton of CaO.

Figure 11 shows that if the demand of lime for OAE is not allowed to increase above the current total capacity of cement plants (right panel), then distance classes are saturated in the expected order. If instead growth is allowed (left panel), all classes other than the first are only temporarily used as the first is scaled up.

Global CCS usage is shown in fig. 12, while in fig. 13 and fig. 14 we report regional CCS usage for the *Main* and *Low CCS* scenarios respectively. It is interesting to notice that in the latter case several regions switch partially or completely towards using CCS for OAE lime production.

Figure 15 shows the growth of the carbon tax across scenarios. It is clear from the left panel that the real-world feasibility and acceptability of the late scenarios is doubtful. In all early scenarios except for *Low CCS*, the carbon tax never exceeds 1000 $\$/GtCO_2$.

Figure 16 shows the mean value of the port capacity constraint (8), which, as observed in the main text, decreases as mitigation is delayed because of the reduction in GDP.

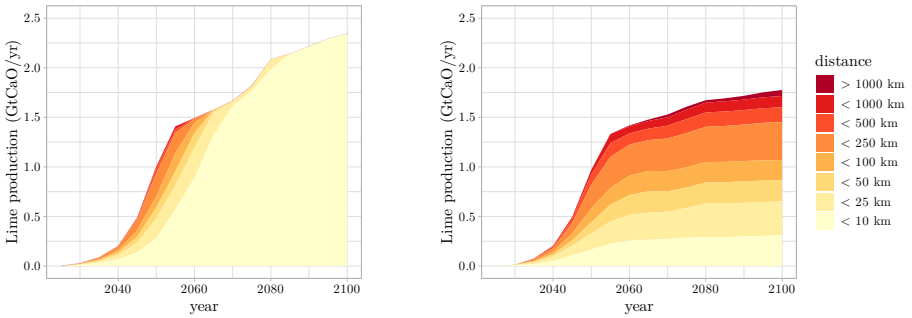
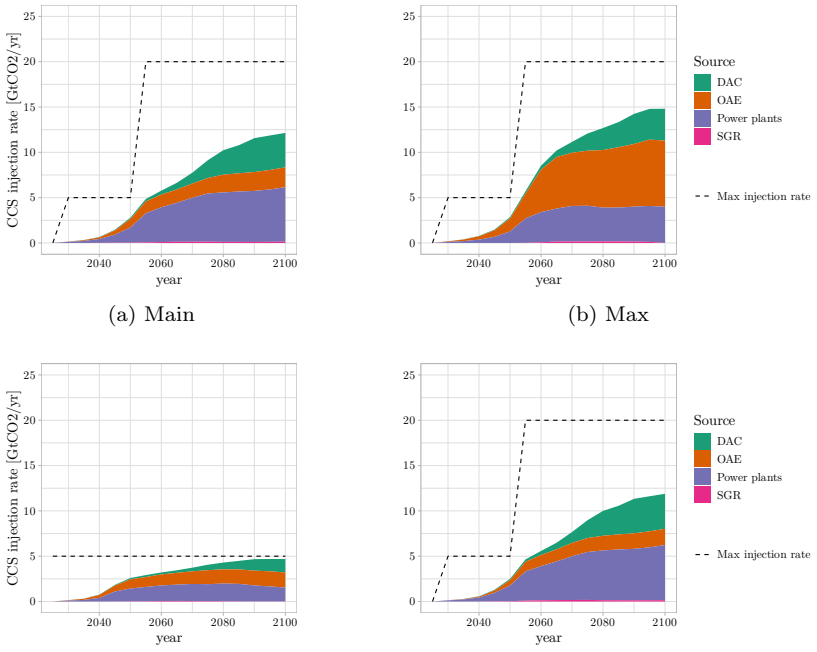


Figure 11: **Lime production** per transport distance class in the main overshoot scenario (left) and in the no mining growth overshoot scenario (right).



(a) Main (b) Max

(c) Low CCS (d) Electric calciner

Figure 12: **CCS utilization.** Global CCS injection rates by source (coloured areas) and limits (dashed lines) in the *Main*, *Max*, *Low CCS*, and *Electric* overshoot scenarios, for the early timing variant. DAC: Direct Air Capture, OAE: calciner emissions, SGR: Steam Gas Reforming.

Figure 17 reports ship utilization by type of ship for the *Max* scenarios. We observe that ship categories generally increase in volume, with the exception of tankers, whose utilization is gradually reduced, likely in connection to decarbonization and switching to renewable sources.

Figure 18 shows the total 2025-2100 emissions from international shipping, including both OAE and the other shipping sectors, and cumulative emissions from fossil fuels and industry (FFI). We observe that differences in emissions

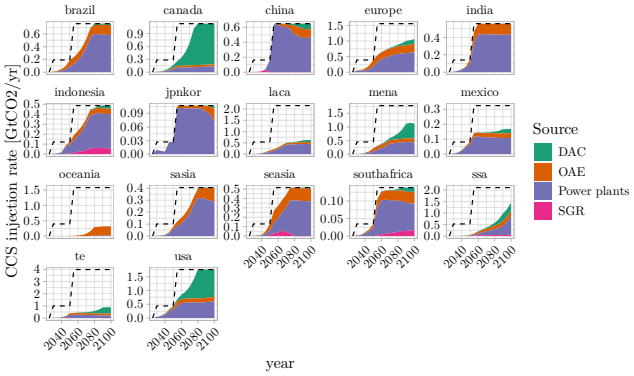


Figure 13: **Regional CCS injection rates** in the early *Main* scenario by source. DAC: Direct Air Capture, OAE: calciner emissions, SGR: Steam Gas Reforming.

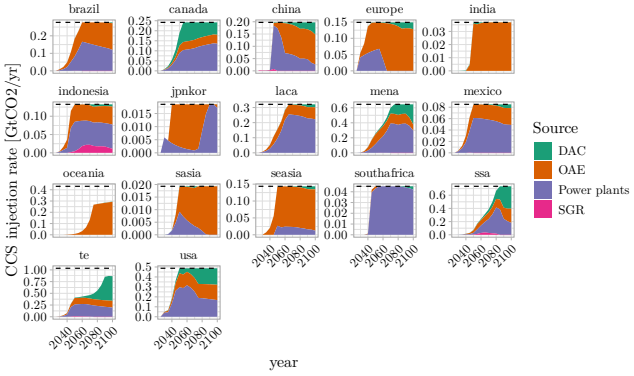


Figure 14: **Regional CCS injection rates** in the early *Low CCS* scenario by source. DAC: Direct Air Capture, OAE: calciner emissions, SGR: Steam Gas Reforming.

from shipping across scenarios at equal timing decrease as mitigation is delayed: excluding the *IMO target* and *Low CCS* scenarios, which are unfeasible for late decarbonization, in the early case CO_2 emissions range from 29 Gt (*No OAE*) to 50 Gt (*No* NH_3), while in the late case they range from 30 Gt to 38 Gt. This is because, if mitigation is delayed, a greater carbon tax is required to meet the emission target, which reduces trade and accelerates shipping decarbonization independently of the other assumptions (see fig. 15; notice in particular the extremely fast carbon tax growth in the late scenarios).

Figure 21 shows the amount of electricity required for the ocean liming process across three scenarios: *Main*, *Max*, and *Electric*. We refer to the main text for a discussion.

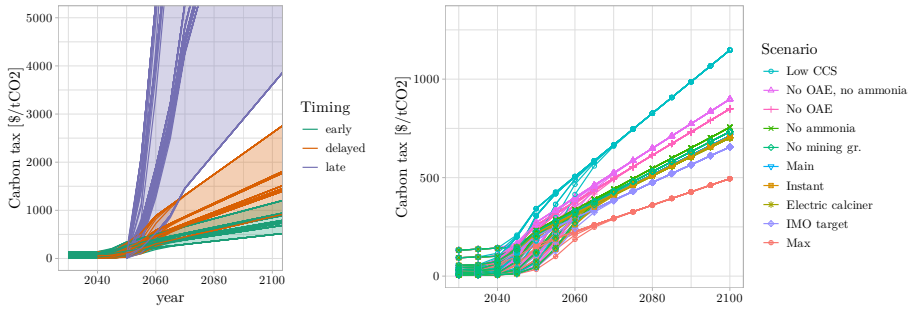


Figure 15: **Carbon tax envelopes** for the different mitigation timings (left) and detail on early scenarios (right). In the right panel, multiple lines are shown for each scenario in early years: each of them corresponds to a region; regional values then converge to a uniform global value.

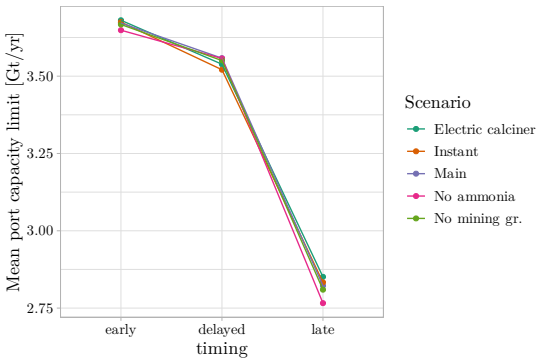


Figure 16: **Port capacity constraint** for the OAE scenarios that are feasible across timings, and excluding the *Max* scenario, where the constraint is not imposed.

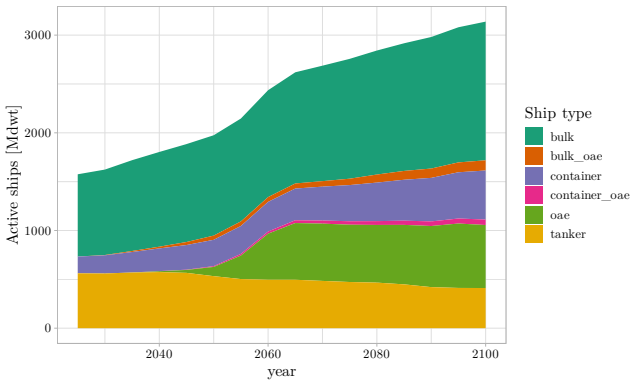


Figure 17: **Ship category breakdown** for the *Max* scenario. 'bulk_oae' and 'container_oae' refer to the additional capacity for OAE on existing bulk carriers and container ships, while 'oae' refers to dedicated ships.

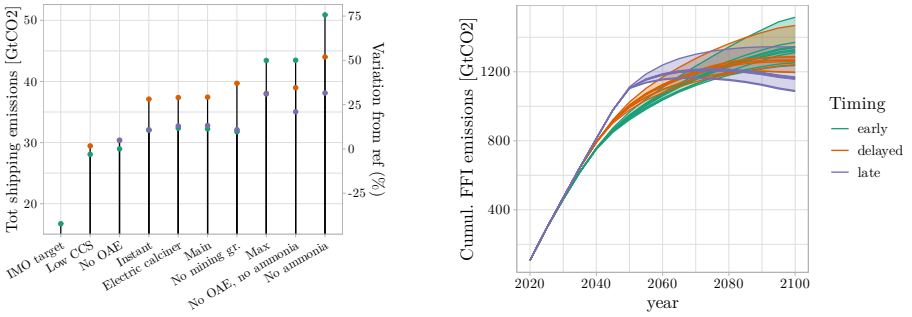


Figure 18: **Shipping emissions**. Total CO_2 emissions from international shipping (left) and cumulative emissions from fossil fuels and industry (right).

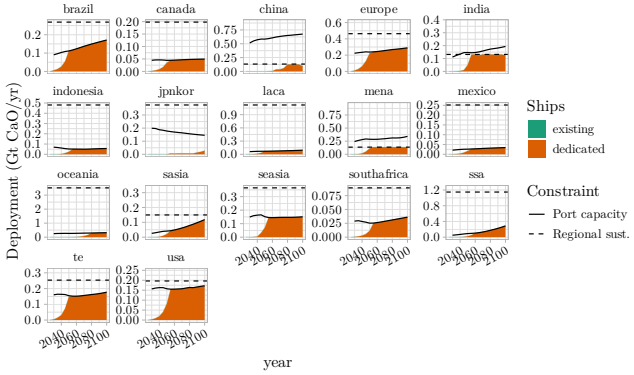


Figure 19: **Deployment and shipping-related constraints** in the early *Main* scenario.

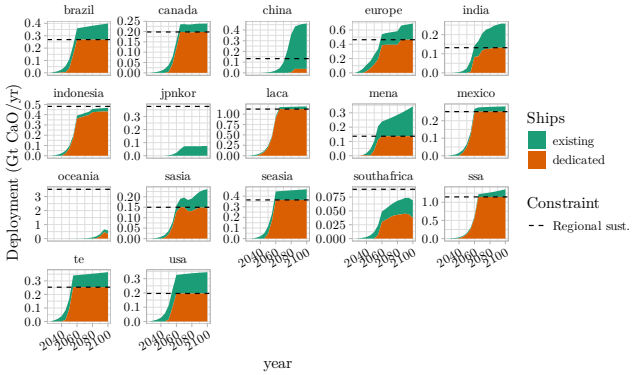


Figure 20: **Deployment and shipping-related constraints** in the early *Max* scenario.

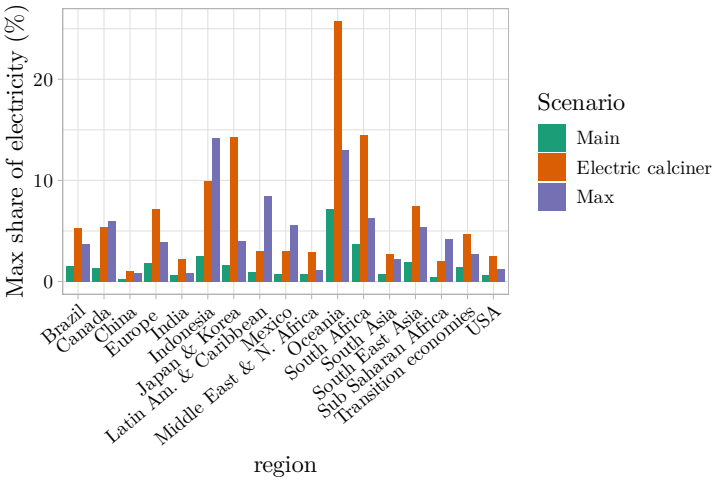


Figure 21: Maximum of the share of electricity usage per region in the *Main*, *Max*, and *Electric* scenarios, with early mitigation, over time.

B.2 Sensitivity to assumed parameters

The parameters used in this study were chosen by relying as much as possible on existing literature. There are, however, two exceptions: factor γ, controlling the maximum yearly amount of material that can be loaded on ships as a fraction of the total trade of a region (see the port capacity constraint (8)), and factor α, controlling the maximum yearly amount of lime that can be produced when OAE is first deployed as a fraction of the present capacity of cement plants (see the scaleup constraint (4)). We assess the sensitivity of OAE removals to these two parameters, and additionally to r_{lime}, the maximum growth rate of the mining industry, appearing in (4).

Results about cumulative gross removal obtained through a $\pm 50\%$ variation in each of the parameters are shown in table 3, while yearly and cumulative removals are reported in fig. 22, fig. 23 and fig. 24.

γ	α	r_{lime}	Total gross removals [GtCO2]
0.20	0.10	0.150	106.150
0.10	0.10	0.150	64.995
0.30	0.10	0.150	137.424
0.20	0.05	0.150	104.913
0.20	0.15	0.150	106.330
0.20	0.10	0.075	90.002
0.20	0.10	0.225	106.129

Table 3: **Results of the sensitivity analysis.**

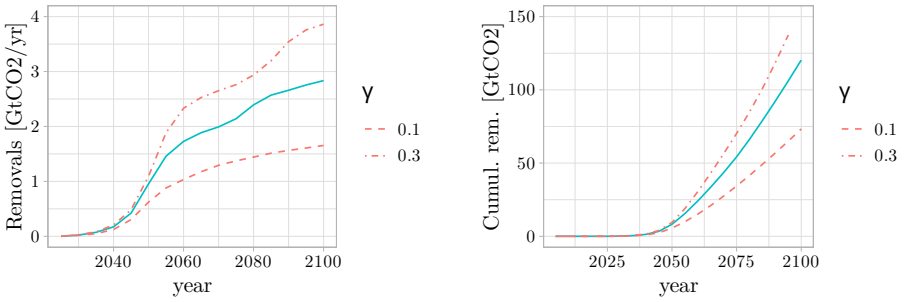


Figure 22: **Influence of port limits.** Sensitivity of yearly gross removals (left) and cumulative gross removals (right) to the port capacity constraint parameter γ.

This analysis shows that a variation of the shipping limit changes significantly the amount of removals. Such variation is nonlinear, as is clear from fig. 22, in the sense that the curves originating from a variation in γ with respect to the *Main* scenarios are not a simple scaling of the latter, showing that the interplay with all other constraints and the modeled system interconnections are key in determining the result.

A negative 50% variation of the mining growth limit (see fig. 24 has an appreciable effect on the result, while a positive variation has no significant effect.

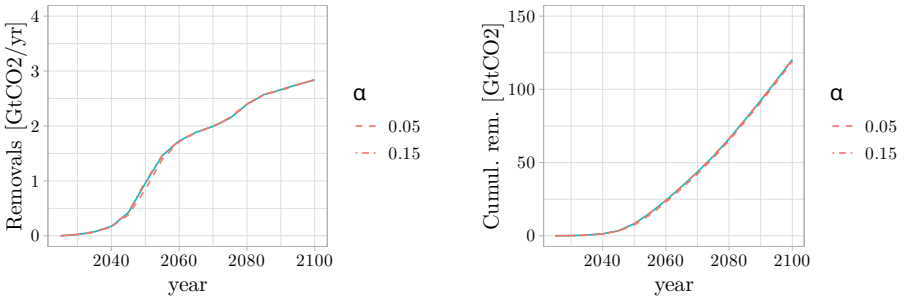


Figure 23: **Influence of initial mining scale.** Sensitivity of yearly gross removals (left) and cumulative gross removals (right) to the initial mining scale parameter α.

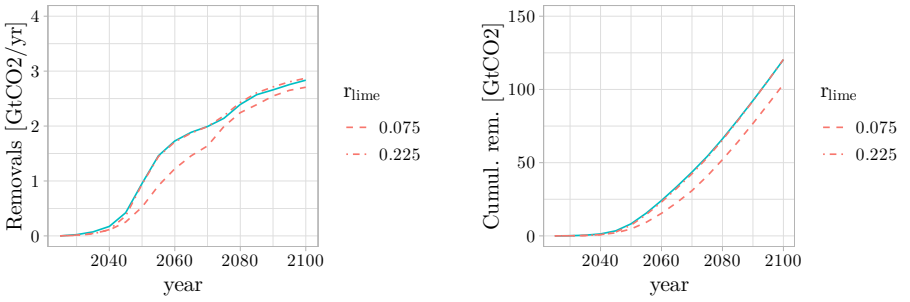


Figure 24: **Influence of mining growth rate.** Sensitivity of yearly gross removals (left) and cumulative gross removals (right) to the mining growth parameter r_{lime}.

On the other hand, a variation of the initial mining limit has very little effect whatever the direction of the variation. This may be counterintuitive, but it is explained by the fact that the coalitions react to a reduction of this upper bound by initially utilizing lime from farther plants, as shown in fig. 25.

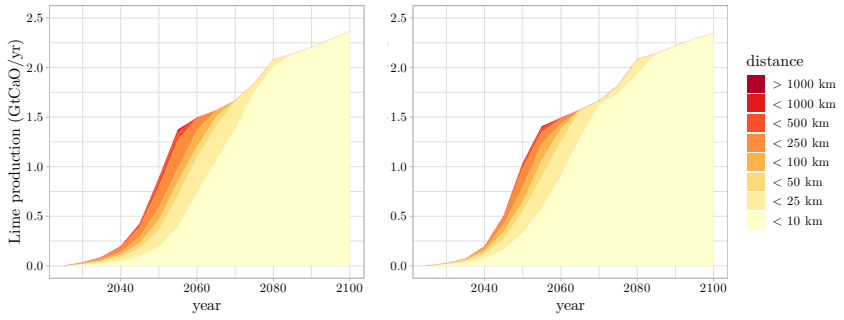


Figure 25: **Production of lime** by distance class from the nearest port with $\gamma = 0.20$ and $\alpha = 0.05$ (left) and $\alpha = 0.15$ (right).

B.3 Climate impacts

Climate impacts were computed as a post-processing step using the RIME code [3]. We selected 6 indicators, 2 from each of the categories reported in [34]:

- Precipitation: consecutive dry days and very heavy precipitation days.
- Hydrology and water resources: drought intensity and water stress index.
- Temperature: heatwave events and cooling degree days.

The RIME framework allows to compute climate impacts either from a temperature input (GWL) or from CO_2 emissions alone. The results of the two approaches for the indicators listed above are reported in fig. 26 and fig. 27, respectively, in terms of fraction of exposed population on a global level. In the first case, we have used the MAGICC climate emulator [22] to compute temperature from WITCH results, considering both GHGs and aerosols.

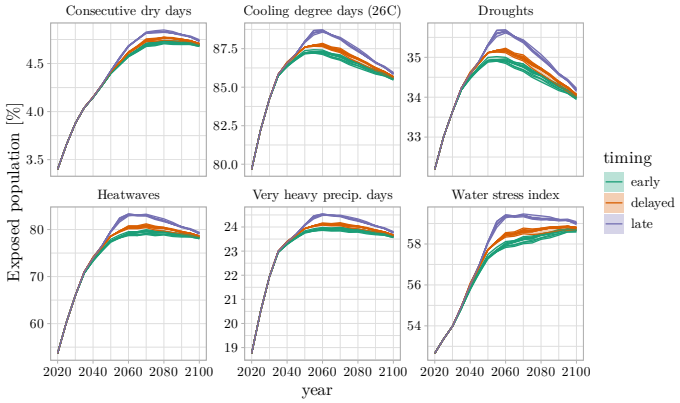


Figure 26: **Climate hazard exposure.** Fraction of world population exposed to each hazard. Full computation using MAGICC+RIME.

RIME also provides an hazard score for each indicator, on a scale of 0 to 6. In fig. 28, we report a composite score computed by summing the scores of all indicators and normalizing to 10. There is a noticeable difference between the two panels of the figure: in case the impacts are assessed from CO_2 emissions only, a clear separation appears between the Main scenarios with OAE and the *No OAE* ones, in that the former are associated to more severe impacts. This is because the availability of the additional CDR capacity results in larger positive emission in the initial time periods of cost-optimal pathways, resulting in higher peak temperatures and longer overshoot. However, in the more comprehensive assessment done using MAGICC, the short-term effects of aerosols partly offset the temperature effect of CO_2 emission reduction, resulting in a more complicated picture in which scenarios with and without OAE do not form two clearly distinct groups with respect to impacts, and have instead comparable values.

In fig. 29 we report again fig. 3c of the main text for the reader's convenience, as it has a visually striking similarity to the first panel of fig. 28. Indeed, as shown on the right in fig. 29, the overshoot indicator can be estimated to very

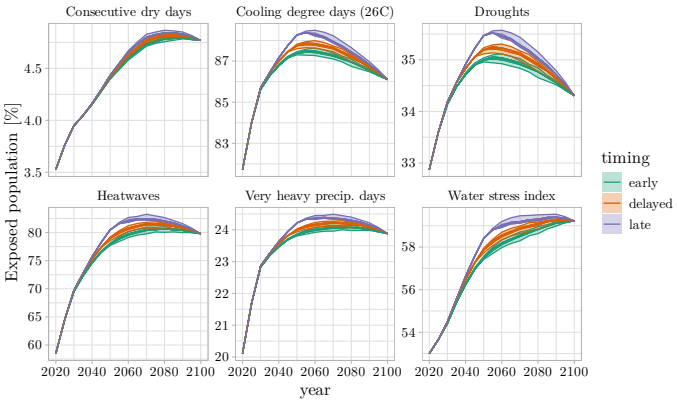
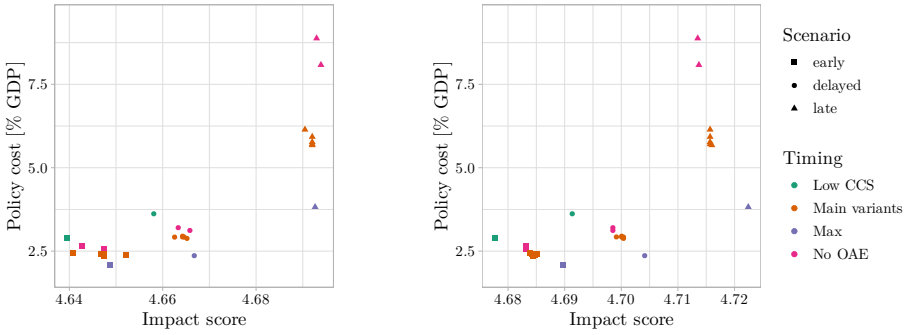


Figure 27: **Climate hazard exposure.** Fraction of world population exposed to each hazard. Simplified computation considering only CO_2 emissions using RIME.



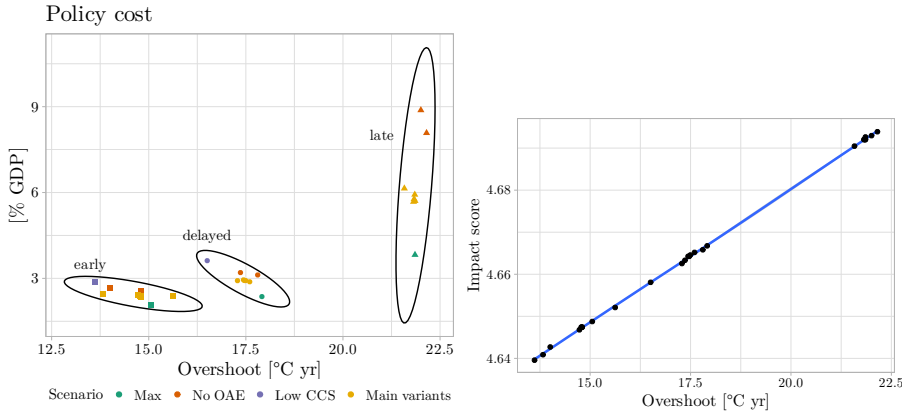
(a) Temperature from MAGICC

(b) Impacts considering CO_2 only

Figure 28: **Summed impact score v. policy cost.**

good approximation as a linear function of the composite impact score. This justifies the definition of the overshoot indicator used in this work.

We remark that the impacts considered here are only triggered by temperature levels, and not by the process of ocean liming itself. Mitigation of direct process impacts is handled in our model by limiting the total amount of lime that can be discharged inside each region's EEZ based on the results of [16], and by assessing that in the *Max* scenario, in which deployment is not limited to EEZs, the total amount of discharged material is within the global limit suggested in [31].



(a) (b)

Figure 29: **Overshoot indicators.** Temperature-years above 1.5°C vs. policy cost (left) and linearity test of the overshoot-impact score relation.

References

[1] World port index (pub 150). `https://msi.nga.mil/Publications/WPI`. Data retrieved on 01/12/2025.

[2] M. Boettcher, K. Brent, H. J. Buck, S. Low, D. McLaren, and N. Mengis. Navigating potential hype and opportunity in governing marine carbon removal. *Frontiers in Climate*, 3, June 2021.

[3] E. Byers, M. Werning, M. Perrette, N. Schwind, V. Krey, K. Riahi, and C.-F. Schleussner. Fast climate impact emulation for global temperature scenarios with the rapid impact model emulator (RIME). *Environmental Research: Climate*, 4(3):035011, Aug. 2025.

[4] K. Calvin, D. Dasgupta, G. Krinner, A. Mukherji, P. W. Thorne, C. Trisos, J. Romero, P. Aldunce, K. Barret, G. Blanco, W. W. Cheung, S. L. Connors, F. Denton, A. Diongue-Niang, D. Dodman, M. Garschagen, O. Geden, B. Hayward, C. Jones, F. Jotzo, T. Krug, R. Lasco, Y.-Y. Lee, V. Masson-Delmotte, M. Meinshausen, K. Mintenbeck, A. Mokssit, F. E. Otto, M. Pathak, A. Pirani, E. Poloczanska, H.-O. Pörtner, A. Revi, D. C. Roberts, J. Roy, A. C. Ruane, J. Skea, P. R. Shukla, R. Slade, A. Slangen, Y. Sokona, A. A. Sörensson, M. Tignor, D. van Vuuren, Y.-M. Wei, H. Winkler, P. Zhai, Z. Zommers, J.-C. Hourcade, F. X. Johnson, S. Pachauri, N. P. Simpson, C. Singh, A. Thomas, E. Totin, A. Alegría, K. Armour, B. Bednar-Friedl, K. Blok, G. Cissé, F. Dentener, S. Eriksen, E. Fischer, G. Garner, C. Guivarch, M. Haasnoot, G. Hansen, M. Hauser, E. Hawkins, T. Hermans, R. Kopp, N. Leprince-Ringuet, J. Lewis, D. Ley, C. Ludden, L. Niamir, Z. Nicholls, S. Some, S. Szopa, B. Trewin, K.-I. van der Wijst, G. Winter, M. Witting, A. Birt, and M. Ha. *IPCC, 2023: Climate Change 2023: Synthesis Report, Summary for Policymakers. Contribution of Working Groups I, II and III to the Sixth Assessment Report of the Intergovernmental Panel on Climate Change [Core Writing Team, H. Lee and J. Romero (eds.)]. IPCC, Geneva, Switzerland.* July 2023.

[5] S. Caserini, D. Pagano, F. Campo, A. Abbà, S. De Marco, D. Righi, P. Renforth, and M. Grosso. Potential of maritime transport for ocean liming and atmospheric CO2 removal. *Frontiers in Climate*, 3, Apr. 2021.

[6] S. Chiquier, A. Gurgel, J. Morris, Y.-H. H. Chen, and S. Paltsev. Integrated assessment of carbon dioxide removal portfolios: land, energy, and economic trade-offs for climate policy. *Environmental Research Letters*, 20(2):024002, Jan. 2025.

[7] J. Emmerling, L. Drouet, L. A. Reis, M. Bevione, L. Berger, V. Bosetti, S. Carrara, E. D. Cian, G. D. M. D'Aertrycke, T. Longden, M. Malpede, G. Marangoni, F. Sferra, M. Tavoni, J. Witajewski-Baltvilks, and P. Havlik. The WITCH 2016 Model - Documentation and Implementation of the Shared Socioeconomic Pathways. Working Paper 2016.42, Fondazione Eni Enrico Mattei, 2016.

[8] European Maritime Safety Agency. Safety of ammonia for use in ships. Final report - Conclusion and recommendations. Technical report, EMSA, Lisbon, 2025.

[9] E. Fernández Villanueva and G. Shaffer. Presentation, calibration and testing of the DCESS II Earth system model of intermediate complexity (version 1.0). *Geoscientific Model Development*, 18(7):2161–2192, Apr. 2025.

[10] Flanders Marine Institute (VLIZ), Belgium. Maritime boundaries geodatabase: Maritime boundaries and exclusive economic zones (200nm), version 12, 2023.

[11] P. M. Forster, C. Smith, T. Walsh, W. F. Lamb, R. Lamboll, C. Cassou, M. Hauser, Z. Hausfather, J.-Y. Lee, M. D. Palmer, K. von Schuckmann, A. B. A. Slangen, S. Szopa, B. Trewin, J. Yun, N. P. Gillett, S. Jenkins, H. D. Matthews, K. Raghavan, A. Ribes, J. Rogelj, D. Rosen, X. Zhang, M. Allen, L. Aleluia Reis, R. M. Andrew, R. A. Betts, A. Borger, J. A. Broersma, S. N. Burgess, L. Cheng, P. Friedlingstein, C. M. Domingues, M. Gambarini, T. Gasser, J. Gütschow, M. Ishii, C. Kadow, J. Kennedy, R. E. Killick, P. B. Krummel, A. Liné, D. P. Monselesan, C. Morice, J. Mühle, V. Naik, G. P. Peters, A. Pirani, J. Pongratz, J. C. Minx, M. Rigby, R. Rohde, A. Savita, S. I. Seneviratne, P. Thorne, C. Wells, L. M. Western, G. R. van der Werf, S. E. Wijffels, V. Masson-Delmotte, and P. Zhai. Indicators of global climate change 2024: annual update of key indicators of the state of the climate system and human influence. *Earth System Science Data*, 17(6):2641–2680, June 2025.

[12] S. Foteinis, J. Andresen, F. Campo, S. Caserini, and P. Renforth. Life cycle assessment of ocean liming for carbon dioxide removal from the atmosphere. *Journal of Cleaner Production*, 370:133309, Oct. 2022.

[13] J. Fuhrman, J. Lane, H. McJeon, G. C. Iyer, M. R. Edwards, Z. Thomas, and J. A. Edmonds. Rate and growth limits for carbon capture and storage. *Environmental Research Letters*, 20(6):064034, May 2025.

[14] M. Gidden, S. Joshi, J. Armitage, A.-B. Christ, M. Boettcher, E. Brutschin, A. Koberle, H. J. Schellnhuber, C.-F. Schleussner, K. Riahi, and J. Rogelj. A prudent planetary boundary for geological carbon storage. May 2025.

[15] M. L. Godec. Global technology roadmap for CCS in industry. sectoral assessment. CO2 enhanced oil recovery. Technical report, United Nations Industrial Development Organization, 2011.

[16] J. He and M. D. Tyka. Limits and CO2 equilibration of near-coast alkalinity enhancement. *Biogeosciences*, 20(1):27–43, Jan. 2023.

[17] IEAGHG. Potential for biomass and carbon dioxide capture and storage. Technical report, 2011.

[18] International Renewable Energy Agency. A pathway to decarbonise the shipping sector by 2050. Technical report, IRENA, Abu Dhabi, 2021.

[19] IPCC. Summary for policymakers. In *Global Warming of 1.5°C. An IPCC Special Report on the impacts of global warming of 1.5°C above pre-industrial levels and related global greenhouse gas emission pathways, in the context of strengthening the global response to the threat of climate change, sustainable development, and efforts to eradicate poverty*, pages 1–24. Cambridge University Press, June 2018.

[20] K. A. Kowalczyk, T. Amann, J. Strefler, M.-E. Vorrath, J. Hartmann, S. De Marco, P. Renforth, S. Foteinis, and E. Kriegler. Marine carbon dioxide removal by alkalinization should no longer be overlooked. *Environmental Research Letters*, 19(7):074033, June 2024.

[21] C. Mack, R. Hanna, D. Dias, and D. Victor. The scalability and carbon removal potential of ocean alkalinity enhancement. Dec. 2025.

[22] M. Meinshausen, S. C. B. Raper, and T. M. L. Wigley. Emulating coupled atmosphere-ocean and carbon cycle models with a simpler model, MAGICC6 – Part 1: Model description and calibration. *Atmospheric Chemistry and Physics*, 11(4):1417–1456, Feb. 2011.

[23] M. J. Mitchell, O. E. Jensen, K. A. Cliffe, and M. M. Maroto-Valer. A model of carbon dioxide dissolution and mineral carbonation kinetics. *Proceedings of the Royal Society A: Mathematical, Physical and Engineering Sciences*, 466(2117):1265–1290, Dec. 2009.

[24] C. A. Moras, L. T. Bach, T. Cyronak, R. Joannes-Boyau, and K. G. Schulz. Ocean alkalinity enhancement – avoiding runaway CaCO3 precipitation during quick and hydrated lime dissolution. *Biogeosciences*, 19(15):3537–3557, Aug. 2022.

[25] Mærsk Mc-Kinney Møller Center for Zero Carbon Shipping. Fuel option scenarios position paper. Technical report, 2021.

[26] H. Naghash, D. Schott, and J. Pruyn. Evolving shipping activity in climate scenarios: Coupling econometrics with integrated assessment model. *Ocean Engineering*, 322:120516, Apr. 2025.

[27] OSRM API. `https://project-osrm.org/docs/v5.5.1/api/#general-options`.

[28] S. Rathod, M. R. Edwards, C. Roy, L. Warnecke, P. Rafaj, G. Kiesewetter, and Z. Klimont. Air quality and health effects of a transition to ammonia–fueled shipping in Singapore. *Environmental Research: Health*, 1(4):041002, Oct. 2023.

[29] P. Renforth and G. Henderson. Assessing ocean alkalinity for carbon sequestration. *Reviews of Geophysics*, 55(3):636–674, July 2017.

[30] J. L. Sarmiento and N. Gruber. *Ocean biogeochemical dynamics*. Princeton University Press, 2006.

[31] J. Strefler, K. Kowalczyk, V. Hofbauer, T. Dorndorf, and L. Baumstark. Ocean liming can help achieve the Paris climate target. *Environmental Research Letters*, 20(9):094004, July 2025.

[32] K. Suselj, D. Carroll, D. Menemenlis, H. Zhang, N. Beatty, A. Savage, and D. B. Whitt. Quantifying regional efficiency of marine carbon dioxide removal (mCDR) via alkalinity enhancement using the ECCO-Darwin ocean biogeochemistry state estimate and an idealized vertical 1-D Model, Mar. 2024.

[33] N. Tkachenko, K. Tang, M. McCarten, S. Reece, D. Kampmann, C. Hickey, M. Bayaraa, P. Foster, C. Layman, C. Rossi, K. Scott, D. Yoken, C. Christiaen, and B. Caldecott. Global database of cement production assets and upstream suppliers. *Scientific Data*, 10(1), Oct. 2023.

[34] M. Werning, D. Hooke, V. Krey, K. Riahi, B. van Ruijven, and E. A. Byers. Global warming level indicators of climate change and hotspots of exposure. *Environmental Research: Climate*, 3(4):045015, Oct. 2024.

[35] D. A. Wolf-Gladrow, R. E. Zeebe, C. Klaas, A. Körtzinger, and A. G. Dickson. Total alkalinity: The explicit conservative expression and its application to biogeochemical processes. *Marine Chemistry*, 106(1–2):287–300, July 2007.

[36] M. Workman, K. Dooley, G. Lomax, J. Maltby, and G. Darch. Decision making in contexts of deep uncertainty - an alternative approach for long-term climate policy. *Environmental Science & Policy*, 103:77–84, Jan. 2020.

[37] R. E. Zeebe and D. Wolf-Gladrow. *CO2 in seawater: equilibrium, kinetics, isotopes*. Amsterdam : Elsevier, 2001.

[38] M. Zhou, M. Tyka, D. Ho, E. Yankovsky, S. Bachman, T. Nicholas, A. Karspeck, and M. Long. Mapping the global variation in the efficiency of ocean alkalinity enhancement for carbon dioxide removal. *Nature Climate Change*, Mar. 2024.